Analytical modeling of laser pulse heating of embedded biological targets: An application to cutaneous vascular lesions

Mirko Mirkov,[a] Evan A. Sherr, and Rafael A. Sierra
Cynosure, Inc., Westford, Massachusetts 01886

Jenifer R. Lloyd
Northeastern Ohio Universities College of Medicine, Rootstown, Ohio 44272

Emil Tanghetti
University of California Davis, School of Medicine, Sacramento, California 95819

(Received 21 October 2005; accepted 23 March 2006; published online 7 June 2006)

Detailed understanding of the thermal processes in biological targets undergoing laser irradiation continues to be a challenging problem. For example, the contemporary pulsed dye laser (PDL) delivers a complex pulse format which presents specific challenges for theoretical understanding and further development. Numerical methods allow for adequate description of the thermal processes, but are lacking for clarifying the effects of the laser parameters. The purpose of this work is to derive a simplified analytical model that can guide the development of future laser designs. A mathematical model of heating and cooling processes in tissue is developed. Exact analytical solutions of the model are found when applied to specific temporal and spatial profiles of heat sources. Solutions are reduced to simple algebraic expressions. An algorithm is presented for approximating realistic cases of laser heating of skin structures by heat sources of the type found to have exact solutions. The simple algebraic expressions are used to provide insight into realistic laser irradiation cases. The model is compared with experiments on purpura threshold radiant exposure for PDL. These include data from four independent groups over a period of 20 years. Two of the data sets are taken from previously published articles. Two more data sets were collected from two groups of patients that were treated with two PDLs (585 and 595 nm) on normal buttocks skin. Laser pulse durations were varied between 0.5 and 40 ms; radiant exposures were varied between 3 and 20 J/cm^2. Treatment sites were evaluated 0.5, 1, and 24 hours later to determine purpuric threshold. The analytical model is in excellent agreement with a wide range of experimental data for purpura threshold radiant exposure. The data collected by independent research groups over the last 20 years with PDLs with wavelengths ranged from 577 to 595 nm were described accurately by this model. The simple analytical model provides an accurate description of a wide range of experimental data. The model can be used to guide the development of future laser designs and help refine laser parameters. © *2006 American Institute of Physics*. [DOI: 10.1063/1.2200592]

I. INTRODUCTION

Understanding the thermal processes in biological targets undergoing laser irradiation continues to be a challenging problem despite the availability and the ever-increasing power of the numerical computational models.[1–6] The high precision of the numerical algorithms is mismatched by the available approximate values of the tissues thermal and optical properties.[7,8] The benefit of analytical models of tissue heating is that the trends produced by variations of the laser pulse parameters can be studied without precise knowledge of all tissue properties. A large number of analytical models derive solutions in terms of infinite sums or integrals that can be evaluated only numerically.[9–12] Although the calculation of these sums or integrals is relatively straightforward using a computer, the clarity of the analytical solution is lost in the process. The assumption that the spatial temperature profile is proportional to the laser fluence profile at all times, has led to a useful time constant model with some limitations and refinements.[13–15] The introduction of specifically chosen temperature profiles in the target at the end of the heating laser pulse have resulted in straightforward theoretical models and important insights for laser treatment of vascular targets.[16–18]

The next logical step to refine the understanding of the target heating process in terms of analytical modeling is to assume specifically chosen spatial and temporal profiles for the heat generation function within the laser target. Pulsed heating of spherical targets by a spatially uniform heater has been solved analytically for a variety of applications.[19,20] Pulsed heating of various target geometries by Gaussian and δ-function sources has been analyzed in Ref. 21 (Chapter 12). The present work shows that it is possible to derive relatively simple closed form analytical solutions of laser pulse heating and subsequent cooling of spherical, cylindrical, and planar biological targets by introducing a few simplifying assumptions. Application of the analytical solutions derived in the case of laser heating of blood vessels has provided direction for improvement in laser design and has led to more effective laser treatment with reduced side

[a]Corresponding author: Mirko Mirkov, Cynosure, Inc., 5 Carlisle Road, Westford, MA 01886; electronic mail: mmirkov@cynosurelaser.com

effects.[22–24] The development of the model presented here follows the general approach of representing the complex process of biological target heating by approximate, but analytically solvable models.

The present work consists of three structural parts. Part one describes the derivation of the analytical model and its application to generalized spherical, cylindrical, and planar targets. Special emphasis is placed on cylindrical targets in the context of application of the model to the treatment of blood vessels by pulsed dye lasers. In the second part, the model is used to compare previously published results of dye laser treatment of small blood vessels.[17,25] The third aspect of this work describes the performance of contemporary pulsed dye lasers in terms of the analytical model.

II. DESCRIPTION OF THE MODEL

The detailed description of the analytical model will be presented in Appendix A only for the case of cylindrical targets. For the cases of planar and spherical targets, shortened descriptions are presented in Appendices B and C.

The thermal analysis presented here is based on a geometry that assumes a cylindrical target of a radius R and infinite length. The target is embedded in an infinite isotropic medium whose thermal properties are identical to those of the target. The target differs from the surrounding medium by the presence of time- and space-dependent heat generation that is concentrated in the target. An example is the case of a target containing a chromophore that results in strong absorption of laser light incident on the target. Heating and cooling of the target are controlled by thermal diffusion. The heat diffusion equation including thermal generation in an isotropic medium is given by

$$\frac{\partial T}{\partial t} - \alpha \nabla^2 T = \frac{h(\vec{r},t)}{\rho c}, \tag{1}$$

where $h(\vec{r},t)$ is the heat generating term and $T(\vec{r},t)$ is the temperature at time t and location $\vec{r}$. The coefficients α, ρ, and c are the thermal diffusivity, density, and heat capacity of the medium and are assumed to be identical inside and outside the cylindrical target. It is assumed that initially the target is at the same temperature as the surrounding medium. The solution of Eq. (1) can be expressed in terms of its Green's function $g(\vec{r},t,\vec{r}',t')$

$$T(\vec{r},t) = \int_{-\infty}^{t} dt' \int_{-\infty}^{\infty}\int_{-\infty}^{\infty}\int_{-\infty}^{\infty} dx'dy'dz' g(\vec{r},t,\vec{r}',t') S(\vec{r}',t'), \tag{2}$$

where $S(\vec{r}',t')=h(\vec{r}',t')/\rho c$ is the source term. The Green's function of Eq. (1) for an infinite isotropic medium is[9]

$$g(\vec{r},t,\vec{r}',t') = \frac{1}{8[\pi\alpha(t-t')]^{3/2}} \exp\left[-\left(\frac{|\vec{r}-\vec{r}'|^2}{4\alpha(t-t')}\right)\right].$$

It is shown in Appendices A, B, and C that the integral in Eq. (2) can be solved analytically in a closed form for a class of heat generation functions of the form

$$h(\vec{r}',t') = Q\Pi(t',\tau)\exp\left(-A\frac{|\vec{r}'|^2}{R^2}\right). \tag{3}$$

The quantity Q describes the heat generation rate at the center of the target. For a rectangular heating pulse of duration τ, depositing energy density q at the center of the target, Q is simply $Q=q/\tau$. For such pulses, the temporal function $\Pi(t',\tau)$ takes the form

$$\Pi(t',\tau) = \theta(t') - \theta(t'-\tau) = \begin{cases} 1 & \text{for } 0 \le t' \le \tau \\ 0 & \text{for } t' > \tau \end{cases},$$

where $\theta(t)$ is the Heaviside step function. $\Pi(t',\tau)$ contains the time dependence of the heating source, a rectangular-shaped temporal pulse of duration τ. The exponential term describes the spatial distribution of the heat generation assumed to have a Gaussian distribution. The free parameter A can be adjusted to account for various degrees of confinement of the heat source within the volume of the target. A very large value of A corresponds to a very localized heating, small values of A describe more diffuse heating.

In most practical cases of interest, there is little knowledge of the heat source distribution within the volume of the target. One common heat source is the case of laser irradiation on biological targets with low to moderate absorption embedded in a tissue environment that exhibits strong scattering. This type of heat source results in nearly uniform heating of the target and deposition of energy density u with units of energy per volume. In this approximation, the heat generation rate Q is chosen so that the total energy deposited by the Gaussian heater considered in Eq. (3) is the same as that deposited by the uniform heater described here. As will be shown, the behavior of biological targets heated nearly uniformly can be described adequately by the above heat source. The expressions derived in appendices (A15), (B5), and (C5) can be used to express the temporal and spatial profiles of the temperature rise in the target. At the center of a cylindrical, spherical, or planar target, the expressions for the temperature rise simplify to

Cylindrical:

$$T_C(t) = \frac{u}{\rho c}\frac{\tau_c}{\tau}\ln\left(\frac{1+A\dfrac{t}{\tau_c}}{1+A\dfrac{\langle t-\tau\rangle}{\tau_c}}\right), \tag{4}$$

Spherical:

$$T_C(t) = \frac{u}{\rho c}\frac{\tau_c}{\tau}\frac{8}{3}\sqrt{\frac{A}{\pi}}\left[\frac{1}{\sqrt{1+A\dfrac{\langle t-\tau\rangle}{\tau_c}}} - \frac{1}{\sqrt{1+A\dfrac{t}{\tau_c}}}\right], \tag{5}$$

Planar:

$$T_C(t) = \frac{u}{\rho c}\frac{\tau_c}{\tau}\frac{4}{\sqrt{\pi A}}\left[\sqrt{1+A\frac{t}{\tau_c}} - \sqrt{1+A\frac{\langle t-\tau\rangle}{\tau_c}}\right], \tag{6}$$

where

$$\langle x \rangle = \begin{cases} x & \text{for } x \geq 0 \\ 0 & \text{for } x < 0 \end{cases}$$

is the Macauley bracket or ramp function, and $\tau_c = R^2/4\alpha = d^2/16\alpha$ is the characteristic time of the target. In the case of a cylindrical or spherical target, d is the target diameter; in the case of a planar target, d is the target thickness.

The target characteristic time τ_c defined here appears to have the same form as the thermal relaxation time τ_r of the target defined in Ref. 16. However, there are a number of important differences between the two. The thermal relaxation time τ_r is defined[16] as the time for an initial Gaussian-shaped temperature distribution at the center of the target to decay to one half of its peak value. Here the characteristic time τ_c arises as a natural time scale in the solution of the thermal diffusion equation and it is not associated with a specified temperature rise or decay. Although the characteristic time τ_c is identical for a cylindrical, spherical, or planar target with characteristic dimension d, their heating and cooling is described by different temporal functions (4)–(6), and there is no assumption of an initial spatial Gaussian temperature profile. Instead of assuming an initial spatial temperature profile, the analysis presented here assumes heat sources with Gaussian spatial profiles.

To complete the description of the approximate Gaussian heat source, the adjustable parameter A must be specified. One convenient choice for the adjustable parameter A is to set it so that the energy deposited by an infinitely short pulse, in any of the three target geometries, will result in nearly the same temperature rise at the center of the target. In the limit of infinitely short pulses, the expressions (4)–(6) reduce to

Cylindrical:

$$T_C(t = \tau \to 0) = \frac{u}{\rho c} A, \tag{7}$$

Spherical:

$$T_C(t = \tau \to 0) = \frac{u}{\rho c} \frac{4}{3\sqrt{\pi}} A^{3/2}, \tag{8}$$

Planar:

$$T_C(t = \tau \to 0) = \frac{u}{\rho c} \frac{2}{\sqrt{\pi}} A^{1/2}. \tag{9}$$

When the same energy density u is deposited in all three targets and the thermal properties ρc are identical, the instantaneous temperature rise becomes a function of the adjustable parameter A. The normalized temperature rise for the three types of targets are plotted in Fig. 1. Ideally the value of the adjustable parameter A would be chosen so that the temperature rises in the three target geometries are the same. However, the plots on Fig. 1 show that is not possible. A temperature discrepancy function can be defined taking the sum of the squared temperature rise differences for each pair of the three types of targets

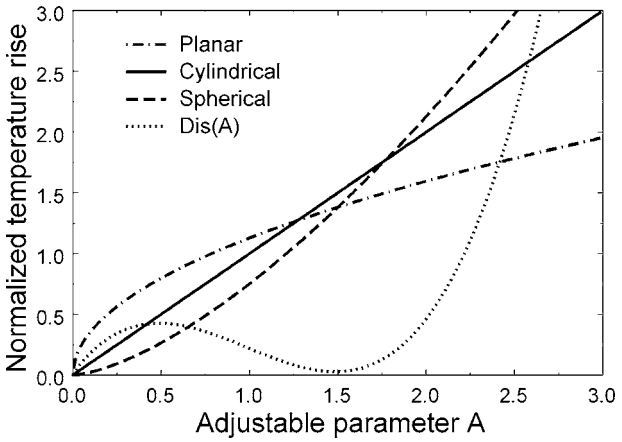

FIG. 1. Peak temperature rises at the center of the three types of targets produced by an infinitely short pulse, Eqs. (7)–(10).

$$Dis(A) = \frac{u}{\rho c}\left[\left(A - \frac{4}{3\sqrt{\pi}}A^{3/2}\right)^2 + \left(A - \frac{2}{\sqrt{\pi}}A^{1/2}\right)^2 + \left(\frac{2}{\sqrt{\pi}}A^{1/2} - \frac{4}{3\sqrt{\pi}}A^{3/2}\right)^2\right] \tag{10}$$

The discrepancy function is plotted also in Fig. 1. The minimum of the discrepancy function can be found by taking its derivative and solving the resulting fourth order equation for $\sqrt{A}$. The two real solutions for A are 0.49 and 1.48, corresponding to the local maximum and minimum. The value $A = 1.48$ minimizes the discrepancy function and that value will be used in the rest of this paper. In general, the choice of an A value would depend on the presence of multiple targets with more than one target geometry. In particular, if there are competing targets with only two different geometries, it would be possible to choose an A value that makes the instantaneous temperature rises identical. However, a fixed value for A for any combination of competing target geometries allows direct comparison of results from different models and that is the approach chosen here.

The Gaussian spatial profile of the heat generating function used here is only an approximation for the actual heat generating profile. A heat generating function peaked in the center of the target would be suitable for a target with a relatively low to moderate absorption coefficient. For highly absorbing targets where most of the light absorption occurs near the periphery of the target, a more suitable heat generating function would be of the Gauss-Hermit type

$$h_2(\vec{r}', t') = Q\Pi(\tau)\frac{r'^2}{R^2}\exp\left(-A_2\frac{r'^2}{R^2}\right). \tag{11}$$

The analytical solution of the Green's function integral (2) for the heat generating function h_2 in cylindrical geometry is outlined in Appendix D.

In principle, the actual heat generating profile can be calculated numerically in a three-dimensional (3D) Monte Carlo program for light propagation. The calculated heat generating profile could then be expanded in terms of Gauss-Hermitian functions of the type (3), (11), and higher order. The resulting analytical solution would be a superposition of the solutions for the individual terms. However, in many

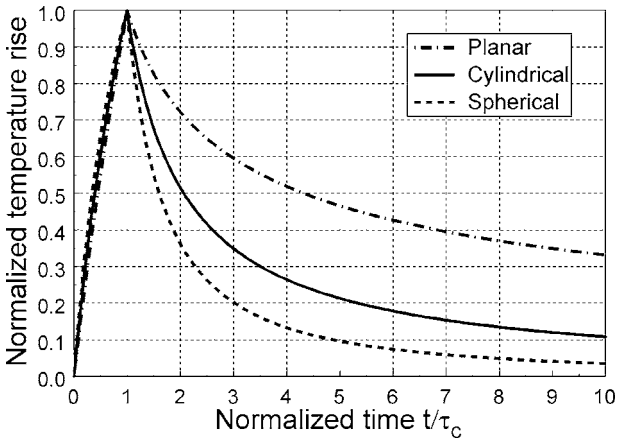

FIG. 2. Evolution of the temperature rise at the center of the three types of targets, Eqs. (4)–(6).

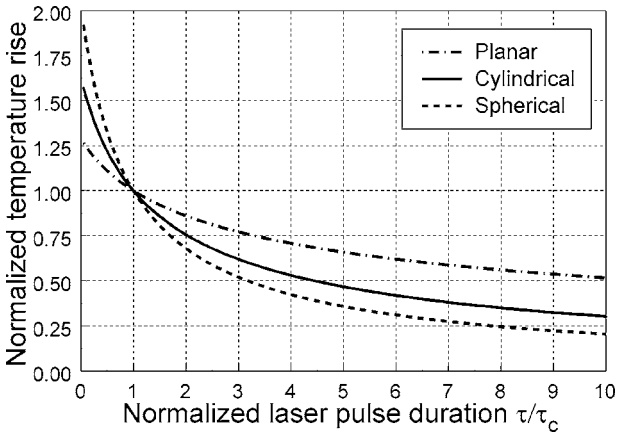

FIG. 3. Peak temperature rise at the end of the laser pulse at the center of the three types of targets, Eqs. (12)–(14).

cases, the solutions obtained from the lowest order terms (3) and (11) are sufficient to analyze the laser pulse heating of the target. Only heat generating functions of the type (3) will be used in the present work and model calculations will be compared with experimental data.

III. SINGLE LASER PULSE HEATING OF EMBEDDED TARGETS

Equations (4)–(6) can be used to illustrate laser pulse heating and subsequent cooling of individual targets. Figure 2 shows the normalized temperature rise at the center of a target plotted versus normalized time t/τ_c for each of the three target geometries. It is assumed that for all targets, the characteristic size R is the same and therefore τ_c is the same. In this example, the laser pulse duration is set to be $\tau=\tau_c$. The temperature rise is normalized for each target type so that at the end of the laser pulse, the temperature rise is equal to 1. This temperature normalization means that the energy density u is different for each target type. The figure shows that during the heating phase $t/\tau_c \leq 1$, the three target types have very similar temporal behavior. However, during the cooling phase $t/\tau_c > 1$ the center of the planar target cools more slowly than the center of the cylindrical target, which in turn cools more slowly than the center of the spherical target. Only the center of the spherical target exhibits a nearly exponential cooling rate of $1/e$ in one characteristic time period. In the subsequent time periods, the cooling of the spherical target slows down and the temperature does not reach $1/e^2$ in two characteristic time periods. The plots in Fig. 2 illustrate the differences between the common simplified assumption of exponential relaxation cooling and the more precise analysis presented here.

In many practical applications, it is of interest to know the peak temperature rise that can be expected in a target when the laser pulse duration is varied. Specifically, it is possible to compare the peak temperature rise of competing biological targets heated by the same laser pulse, for example, cylindrical blood vessels and planar epidermis. Equations (4)–(6) can be used to derive the peak temperature rise at the center of the target at the end of a laser pulse of duration τ, $t=\tau$,

Cylindrical:

$$T_C(t=\tau)=\frac{u}{\rho c}\frac{\tau_c}{\tau}\ln\left(1+A\frac{\tau}{\tau_c}\right), \tag{12}$$

Spherical:

$$T_C(t=\tau)=\frac{u}{\rho c}\frac{\tau_c}{\tau}\frac{8}{3}\sqrt{\frac{A}{\pi}}\left[1-\frac{1}{\sqrt{1+A\frac{\tau}{\tau_c}}}\right], \tag{13}$$

Planar:

$$T_C(t=\tau)=\frac{u}{\rho c}\frac{\tau_c}{\tau}\frac{4}{\sqrt{\pi A}}\left[\sqrt{1+A\frac{\tau}{\tau_c}}-1\right]. \tag{14}$$

The normalized temperature rise at the center of each target is plotted in Fig. 3 versus normalized laser pulse duration τ/τ_c. For all targets, the τ_c is the same. The temperature rise is normalized for each target type so that when the laser pulse duration is equal to the characteristic time, $\tau=\tau_c$, the temperature rise is equal to 1. The plots on Fig. 3 show that the present model leads to finite temperature rise even for infinitely short pulses. The magnitude of the temperature rise produced by an infinitely short pulse is calculated using equations (7)–(9). The variation of the pulse duration has the largest effect on the peak temperature rise for the case of a spherical target and the least effect for the case of a planar target geometry. For a planar target, the laser pulse duration τ has to be more than ten times longer than τ_c if the peak temperature in the target is to be kept to less than $1/2$ of its value when $\tau=\tau_c$.

IV. HEATING OF EMBEDDED CYLINDRICAL TARGETS BY COMPOUND LASER PULSES

Laser systems used to heat biological targets often emit pulse sequences of individual subpulses each of duration τ_s grouped into a compound heating pulse of total duration τ_p. The formalism developed in this work can be expanded to include target heating by such compound pulses. Only the case of compound pulse heating of cylindrical targets will be discussed here. The formulas for the heating of planar and spherical targets can be derived in a similar fashion.

The temporal profile of a compound pulse of duration τ_p consisting of n identical individual subpulses each of duration τ_s can be described by the function

$$\Pi_n(t',\tau_s,\tau_p)=\frac{1}{n}\sum_{j=0}^{n-1}\Pi\left(t'-j\frac{\tau_p-\tau_s}{n-1},\tau_s\right). \tag{15}$$

The normalization factor $\frac{1}{n}$ is included in the expression for the temporal profile so that for any number of individual subpulses within a compound pulse, the total energy delivered by the compound pulse remains the same. The factor $(\tau_p-\tau_s)/(n-1)$ describes the time delay between the subsequent subpulses of duration τ_s when n individual subpulses form a compound pulse of duration τ_p.

The heat generating function with temporal profile defined by Eq. (15) can be substituted in the derivation for cylindrical geometry in Appendix A to obtain the temperature inside a cylindrical target heated by a compound pulse

$$T_n(r,t)=\frac{u}{\rho c}\frac{\tau_c}{n\tau_s}\sum_{j=0}^{n-1}\left[E_1\left(\frac{r^2}{R^2}\frac{A}{1+A\dfrac{\left\langle t-j\dfrac{\tau_p-\tau_s}{n-1}\right\rangle}{\tau_c}}\right)-E_1\left(\frac{r^2}{R^2}\frac{A}{1+A\dfrac{\left\langle t-j\dfrac{\tau_p-\tau_s}{n-1}-\tau_s\right\rangle}{\tau_c}}\right)\right].$$

The constants ρ and c are defined following Eq. (1), the definition of u precedes Eq. (4), and $E_1(s)$ is the exponential integral defined in Appendix A. At the center of the cylindrical target, the last expression simplifies to

$$T_{nC}(t)=\frac{u}{\rho c}\frac{\tau_c}{n\tau_s}\sum_{j=0}^{n-1}\left[\ln\left(\frac{1+A\dfrac{\left\langle t-j\dfrac{\tau_p-\tau_s}{n-1}\right\rangle}{\tau_c}}{1+A\dfrac{\left\langle t-j\dfrac{\tau_p-\tau_s}{n-1}-\tau_s\right\rangle}{\tau_c}}\right)\right]. \tag{16a}$$

The last formula can be rearranged so that instead of a sum of logarithms, it is expressed as the logarithm of a product

$$T_{nC}(t)=\frac{u}{\rho c}\frac{\tau_c}{n\tau_s}\ln\left[\prod_{j=0}^{n-1}\left(\frac{1+A\dfrac{\left\langle t-j\dfrac{\tau_p-\tau_s}{n-1}\right\rangle}{\tau_c}}{1+A\dfrac{\left\langle t-j\dfrac{\tau_p-\tau_s}{n-1}-\tau_s\right\rangle}{\tau_c}}\right)\right]. \tag{16b}$$

The expression (16b) allows for easy verification that when the compound pulse reduces to a single pulse, that is when $\tau_p=n\tau_s$, all but the zeroth and the last terms in the product cancel and Eq. (16b) reduces to Eq. (4) for a single pulse of duration τ_p.

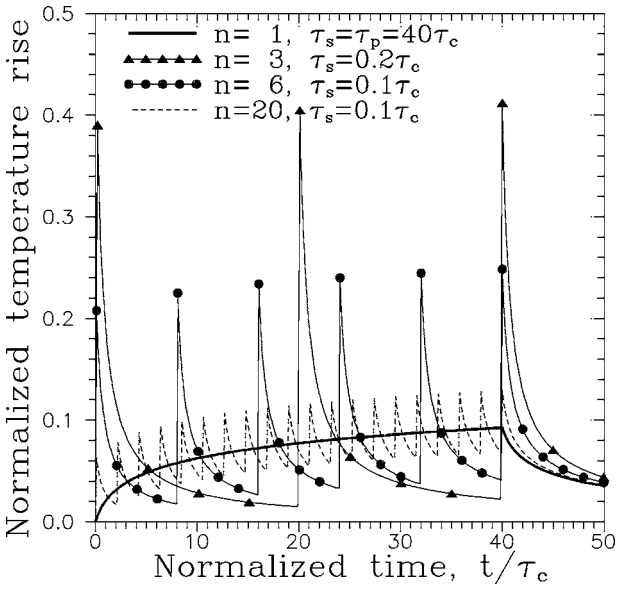

FIG. 4. Evolution of the temperature rise at the center of a cylindrical target, Eq. (16), for various pulse formats. In all cases, the deposited energy density is the same and the total pulse duration is the same $\tau_p=40\tau_r$.

The expression for the temperature rise at the center of a cylindrical target heated by a compound pulse, Eq. (16), provides insight into the heating of cylindrical targets by compound pulses. Figure 4 shows the normalized temperature rise at the center of the target plotted versus normalized time t/τ_c. The temperature rise is normalized, so that heating with a laser pulse that consists of only one pulse of duration $\tau_p=\tau_s=0.5\tau_c$, results in a temperature rise equal to 1. In all the pulse formats illustrated in Fig. 4, the compound pulse duration is the same, $\tau_p=40\tau_c$. All the compound pulses shown deliver the same total energy. The figure illustrates a benefit of multipulse heating. During the time interval between the individual subpulses, the target partially cools off and its peak temperature remains lower than the peak temperature corresponding to a single short pulse of the same energy. A single long pulse of duration $\tau_p=\tau_s=40\tau_c$ would result in an even lower target temperature; however, such pulses may be impractical for generation with certain types of lasers such as the pulsed dye laser.

Figure 4 shows a general trend. When the number of subpulses increases, the peak temperature in the target decreases. This is demonstrated in Fig. 5. Here the peak temperature at the end of the pulse, $t=\tau_p$, is plotted as a function of the number of subpulses. The curve labeled $\tau_c=0.025\tau_p$ summarizes the trend observed in Fig. 4. The dashed line represents the lowest value of the peak temperature that is achieved when a sufficiently large number n of subpulses is included, so that $n\tau_s=\tau_p$ and the effect of the compound pulse approaches that of a single pulse of duration τ_p. The rest of the curves apply to targets with larger τ_c, and therefore larger diameters. It becomes clear from Fig. 5 that a key benefit of compound pulse heating is the possibility to heat simultaneously using the same laser pulse targets of varying diameters and to achieve higher central temperatures in the

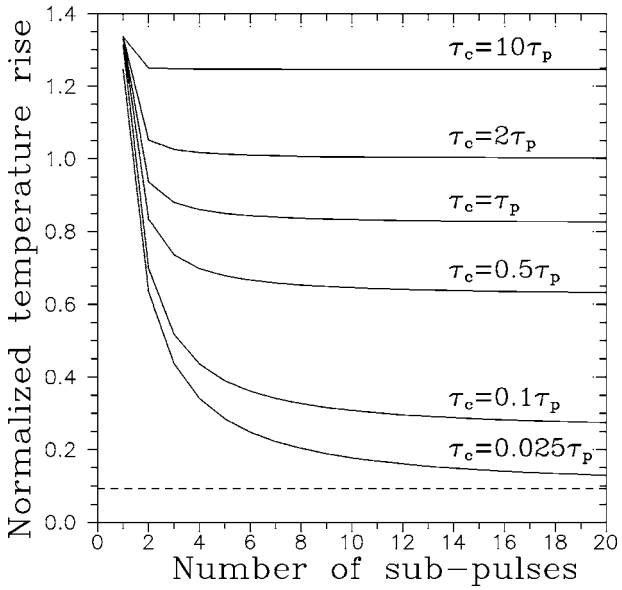

FIG. 5. Peak temperature at the center of cylindrical targets, Eq. (16), with various diameters, $\tau_c=d^2/16\alpha$. In all cases, the total pulse duration and the deposited energy density are the same and the individual subpulse duration is the same $\tau_s=0.0025\tau_p$.

larger targets and lower central temperatures in the smaller targets. Increasing the number of subpulses is especially beneficial when the characteristic time of the small target τ_c is much shorter than the laser pulse duration τ_p.

Simultaneous heating of targets with varying sizes (and characteristic times τ_c) is illustrated on Fig. 6. The larger targets accumulate the heat from the individual subpulses more effectively and achieve higher peak temperature than the temperature in the smaller targets. In the smaller targets where τ_c is much shorter than τ_p ($\tau_c=0.025\tau_p$), the heat deposited in the target dissipates during the time interval between individual subpulses and the peak temperature is only slightly higher than the peak temperature resulting from

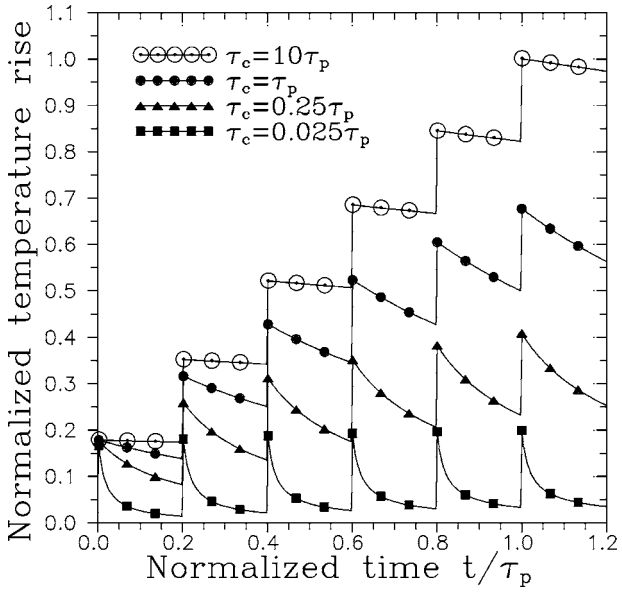

FIG. 6. Evolution of the temperature rise at the center of cylindrical targets, Eq. (16), with various diameters. In all cases, the individual subpulse duration is the same $\tau_s=0.0025\tau_p$.

heating by an individual subpulse. In larger targets where τ_c is longer than τ_p ($\tau_c=10\tau_p$), the target accumulates the heat deposited by individual subpulses and its peak temperature is only slightly lower than the peak temperature that would be observed if all the energy were deposited by a single subpulse.

V. VERIFICATION OF THE ANALYTICAL MODEL USING EXPERIMENTAL RESULTS: APPLICATION TO THE HEATING OF BLOOD VESSELS

The analytical model presented here predicts the temperature rise that occurs in embedded biological targets as a function of the tissue characteristics and the specifications of a heating laser pulse. In most practical cases, the temperature of the embedded target cannot be measured directly, making a direct comparison of the model with experimental data difficult. However, even without temperature measurements, a comparison is possible using a few simplifying assumptions.

The formulas for the temperature rise at the center of cylindrical targets imply a linear dependence on the deposited energy density u and a nonlinear dependence on the pulse duration. In most practical applications for cylindrical target heating, the pulse duration is well known. However, the energy density deposited in the target u (J/cm^3) cannot be measured directly but only can be calculated approximately by means of a Monte Carlo scattering model or light transport formalism. Any approach to the calculation of the energy density u necessitates a set of assumptions about the scattering and absorption properties of the skin structures.

In the absence of nonlinear optical effects, the energy density delivered in the target is directly proportional to the radiant exposure delivered to the skin. However, the proportionality coefficient can be calculated only approximately. The approximate calculation of the deposited energy density u can be avoided by comparing the temperature rise calculated for various pulse formats with the temperature rise calculated for a pulse format that produces a well-established tissue effect. That approach contains the implicit assumption that the most important characteristic for the tissue damage process is the peak temperature that was achieved. An alternative is to use the damage integral formalism that takes into account the complete temporal dependence of the temperature rise. However, that involves the calculation of integrals containing imprecise experimentally measured parameters. The simpler peak temperature approach is used in the present work and it will be shown to yield simple and insightful results.

Clinically, purpura is a side effect often observed in dermatological treatments involving dye lasers. Purpura manifests as a coagulation of small vessels in the laser treated area on the skin. Purpura may last a few days to a few weeks and is an unwelcome transient cosmetic side effect. The radiant exposure level that triggers purpura is a function of various laser parameters and has been reported in numerous publications.[17,25] The purpura threshold fluence (THF) defined in Ref. 17 is equivalent to the purpura threshold radiant exposure (PTRE) used in the present work. The radiant exposure is defined as the delivered energy density per unit

area and characterizes the laser system, while the fluence is the energy density of the laser beam in the tissue, as defined in Chapter 2 of Ref. 21. Although there is a clear distinction between THF and PTRE, typically in clinical publications purpura threshold fluence is used instead of PTRE.

The purpura observed with dermatological laser applications provides a suitable tissue effect that can be used to compare our analytical model with experimental results. The use of clinical purpura as a benchmark tissue effect is possible because it is caused by thermal damage to blood vessels that can be considered as cylindrical targets.[17,25] The use of purpura as an indicator assumes that for any pulse format and any blood vessel diameter, thermal damage resulting in purpura will occur at the same temperature T_p. The value of T_p can be estimated from clinical studies, but it is not needed. Instead, it is assumed that regardless of vessel topology, once T_p is reached, purpura occurs. This results in a simple but powerful means of describing clinical data analytically as will be demonstrated.

VI. COMPARISON WITH CLINICAL DATA USING SINGLE LASER PULSE FOR HEATING OF BLOOD VESSELS

The expression describing the peak temperature observed in an embedded cylindrical target as a result of single pulse heating (12) can be rearranged to solve for the deposited energy density u_p required to achieve purpura. u_p is a function of the purpura threshold temperature T_p and the laser pulse duration τ

$$u_p(d,\tau) = \rho c T_p \frac{\tau}{\tau_c} \frac{1}{\ln\left(1 + A\frac{\tau}{\tau_c}\right)}. \tag{17}$$

In the linear approximation, the energy density deposited in the target u is proportional to the radiant exposure delivered on the surface of the skin F. Therefore Eq. (17) can be used to express the threshold radiant exposure F_p that will cause clinical purpura

$$F_p(d,\tau) = \gamma \frac{\tau}{\tau_c} \frac{1}{\ln\left(1 + A\frac{\tau}{\tau_c}\right)}. \tag{18}$$

The proportionality coefficient γ is a function of T_p and the optical and thermal properties of the skin and the target vessel (assumed to be constant). Equation (18) can be evaluated for any combination of laser pulse duration and vessel diameter. The results can be compared with existing clinical data in the literature.

The expression for the PTRE (18) was used to analyze the expansive set of experimental data on selective vascular injury resulting from laser irradiation with a 577 nm dye laser.[25] The experimental data points from the study[25] are plotted on Fig. 7 along with their error bars. In that study, purpura thresholds were determined for laser pulse durations covering three orders of magnitude. On the same figure, the solid line represents the least squares fit of Eq. (18) to the data points. The least squares fit was done with γ and τ_c treated as adjustable parameters. The calculated value for

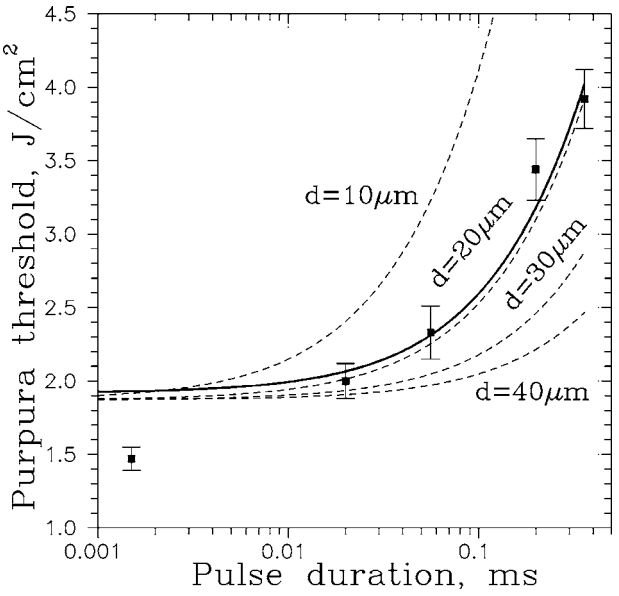

FIG. 7. Purpura threshold radiant exposure versus pulse duration. Experimental data points with error bars are from Ref. 25 The solid line is the theoretical best fit line, Eq. (18), dashed lines are model calculations, Eq. (20). Wavelength=577 nm.

$\tau_c \approx 0.2$ ms corresponds to a target diameter $d \approx 20$ μm. Histology has shown that this is a typical diameter for the normal capillaries damaged in the purpura threshold study. There is a remarkably good agreement between the theoretical model (the solid line) and the experimental data for all pulse durations between 20 μs and 360 μs.

The analytical calculation does not fit the experimental data for the 1.5 μs pulse duration. However, at this short pulse duration, the histological studies exhibited evidence of shattered vessels that was probably due to vaporization. The analytical thermal model presented here does not include the possibility for a phase change in the target; this may explain the difference in the calculated and experimental damage threshold radiant exposure at the 1.5 μs pulse duration.

The normal capillaries damaged in a typical purpura threshold study have a range of diameters between 10 and 40 μm.[25] The analytical model shows a very good fit with the experimental data when the target diameter is 20 μm. The model can be expanded to calculate the purpuric threshold for the whole range of 10 to 40 μm. The experimentally measured purpuric threshold of 3.92 J/cm^2 for 360 μs pulses will be used as reference PTRE, F_{pe}=3.92 J/cm^2, for the reference pulse duration τ_{pe}=360 μs. The reference 20 μm vessels have characteristic time τ_{c20}. The purpuric peak temperature rise T_p is assumed to be the same for any vessel diameter

$$T_p(t=\tau) = \frac{u_p}{\rho c}\frac{\tau_c}{\tau}\ln\left(1 + A\frac{\tau}{\tau_c}\right) = \frac{u_{pe}}{\rho c}\frac{\tau_{c20}}{\tau_{pe}}\ln\left(1 + A\frac{\tau_{pe}}{\tau_{c20}}\right). \tag{19}$$

In the linear approximation, the energy density deposited in the target u is proportional to the radiant exposure delivered on the surface of the skin F. Therefore, the last equation can be rewritten for the PTREs F_p and F_{pe}

$$F_p(d,\tau) = F_{pe}\frac{\tau}{\tau_c}\frac{\tau_{c20}}{\tau_{pe}}\frac{\ln\left(1+A\frac{\tau_{pe}}{\tau_{c20}}\right)}{\ln\left(1+A\frac{\tau}{\tau_c}\right)}. \quad (20)$$

The PTREs calculated from Eq. (20) are shown in Fig. 7 as dashed lines. The calculated plots for the 20 μm vessels based on Eq. (20)—dashed line and least squares fit of Eq. (18)—solid line are both in very good agreement with the experimental data. That agreement confirms the assumption that the clinical PTREs can be used as a benchmark to apply the analytical model to clinical experiments. All the calculated plots show similar PTRE for shorter pulse durations and progressively larger differences as the pulse duration increases. That would be expected because for shorter pulse durations, the heat is confined in the vessels and produces similar temperature raises, coagulation, and purpura. For longer pulse durations, the heat transfer from the smaller vessels is faster and that leads to higher purpura thresholds.

VII. COMPARISON WITH CLINICAL DATA USING TWO LASER SUBPULSES FOR HEATING OF BLOOD VESSELS

The initial clinical study of blood vessel damage by compound laser pulses explored a two subpulse treatment of port-wine stain microvessels.[17] Two 585 nm dye lasers were combined to fire a two subpulse heating pulse. The interval between the subpulses and their amplitudes were varied.[17] In this study, initially the PTRE was determined for a single pulse treatment. Next, in the two subpulse treatment, the leading pulse was set at 80% of the single pulse PTRE, and the delay and amplitude of the second pulse were varied to determine the PTRE of the compound pulse as a function of the delay between subpulses.

The expression for the temperature of embedded cylindrical targets due to multi-sub-pulse heating (16a) can be rewritten to describe two subpulses of unequal energy deposition. The purpuric temperature rise T_{2p} at the end of the two subpulse compound pulse is

$$T_{2p}(t=\tau_p) = \frac{1}{\rho c}\frac{\tau_c}{\tau_s}\left[u_1 \ln\left(\frac{1+A\frac{\tau_p}{\tau_c}}{1+A\frac{\tau_p-\tau_s}{\tau_c}}\right) + u_2 \ln\left(1+A\frac{\tau_s}{\tau_c}\right)\right]. \quad (21)$$

Equation (21) can be written in the notation used in Ref. 17 by substituting the pulse delay $\Delta t=\tau_p-\tau_s$. The single subpulse temperature rise that would cause purpura, T_p, is expressed from Eq. (12)

$$T_p(t=\tau) = \frac{u_p}{\rho c}\frac{\tau_c}{\tau_s}\ln\left(1+A\frac{\tau_s}{\tau_c}\right). \quad (22)$$

Following the assumption that the purpura threshold temperature rise is the same for any pulse format, $T_p=T_{2p}$, Eqs. (21) and (22) are reduced to a single expression

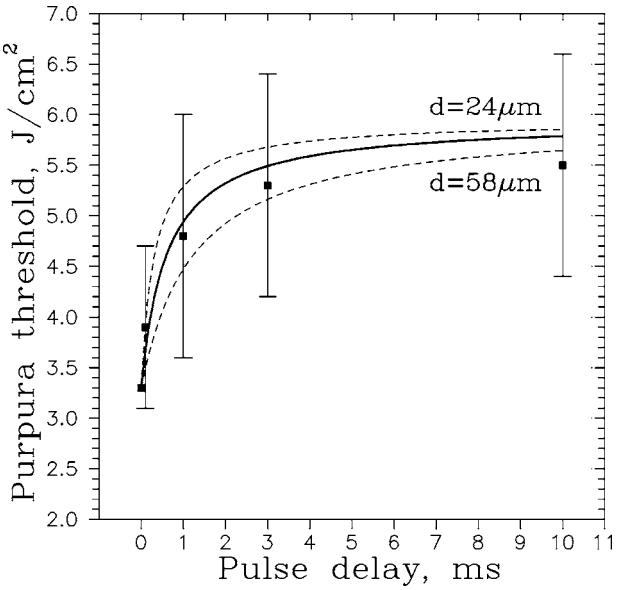

FIG. 8. Dual pulse purpura threshold radiant exposure versus pulse delay. Experimental data points with error bars are from Ref. 17. Solid line is the theoretical calculation, Eq. (24), for the mean vessel diameter $d=37.5$ μm. Wavelength=585 nm.

$$u_p \ln\left(1+A\frac{\tau_s}{\tau_c}\right) = u_1 \ln\left(\frac{1+A\frac{\Delta t+\tau_s}{\tau_c}}{1+A\frac{\Delta t}{\tau_c}}\right) + u_2 \ln\left(1+A\frac{\tau_s}{\tau_c}\right). \quad (23)$$

In the linear approximation, the energy density deposited in the target is proportional to the radiant exposure delivered on the surface of the skin, and Eq. (23) can be written for the radiant exposures F_p, F_1, and F_2. In the clinical study,[17] the radiant exposure delivered in the leading subpulse was set to 80% of the PTRE, $F_1=0.8F_p$. The total PTRE delivered by the dual pulse is $F_T=F_1+F_2=0.8F_p+F_2$. Using Eq. (23), F_T can be expressed as

$$F_T(\Delta t) = F_p\left[1.8-0.8\frac{\ln\left(\frac{1+A\frac{\Delta t+\tau_s}{\tau_c}}{1+A\frac{\Delta t}{\tau_c}}\right)}{\ln\left(1+A\frac{\tau_s}{\tau_c}\right)}\right]. \quad (24)$$

The expression for the total PTRE shows that for any pulse delay Δt, F_T cannot exceed 180% of the single pulse purpura threshold F_p. All the quantities needed to calculate Eq. (24) are provided in Ref.17, $F_p=3.3$ J/cm^2, $\tau_s=0.36$ ms, and blood vessel diameters between 24 and 58 μm with mean value of 37.5 μm. Figure 8 shows a plot of Eq. (24) for $d=37.5$ μm as a solid line. The two dashed lines on the same plot correspond to the full range of blood vessel diameters observed in the clinical study. Agreement between the analytical model and the experimental data is very good over the entire range of subpulse delay intervals considered in the study.

VIII. MULTI SUBPULSE LASER HEATING OF BLOOD VESSELS

The concept of increasing the PTRE from a single pulse to two subpulses can be expanded to extended pulse formats consisting of three or more subpulses. The analytical model presented here can be applied to calculate the PTRE of such compound pulses.

The expression for the temperature of embedded cylindrical targets due to multi-sub-pulse heating (16) can be rewritten for the purpuric temperature rise T_{np} that is reached at the end of the compound pulse $t=\tau_p$

$$T_{np}(t=\tau_p) = \frac{u_n}{\rho c}\frac{\tau_c}{n\tau_s}\ln\left[\prod_{j=0}^{n-1}\left(\frac{1+A\dfrac{(n-j-1)\tau_p+j\tau_s}{(n-1)\tau_c}}{1+A\dfrac{(n-j-1)}{(n-1)}\dfrac{(\tau_p-\tau_s)}{\tau_c}}\right)\right]. \tag{25}$$

Here u_n is the total energy density delivered by the sequence of n subpulses.

The single pulse temperature rise that would cause purpura by predominant coagulation of 20 μm vessels, T_p, is expressed from Eq. (12)

$$T_p(t=\tau) = \frac{u_p}{\rho c}\frac{\tau_{c20}}{\tau_b}\ln\left(1+A\frac{\tau_b}{\tau_{c20}}\right). \tag{26}$$

Here τ_b is the duration of the single pulse used as a benchmark for clinical purpura and τ_{c20} is the characteristic time for a 20 μm vessel. Following the assumption that the purpura threshold temperature rise is the same for any pulse format, $T_{np}=T_p$, Eqs. (25) and (26) are reduced to

$$u_p\frac{\tau_{c20}}{\tau_b}\ln\left(1+A\frac{\tau_b}{\tau_{c20}}\right) = u_n\frac{\tau_c}{n\tau_s}\ln\left[\prod_{j=0}^{n-1}\left(\frac{1+A\dfrac{(n-j-1)\tau_p+j\tau_s}{(n-1)\tau_c}}{1+A\dfrac{(n-j-1)}{(n-1)}\dfrac{(\tau_p-\tau_s)}{\tau_c}}\right)\right]. \tag{27}$$

In the linear skin optic approximation, the energy density deposited in the target is proportional to the radiant exposure delivered on the surface of the skin, and Eq. (27) can be rewritten for the single pulse PTRE F_p and the multipulse PTRE F_n

$$F_n(d,\tau_s,\tau_p,n) = F_p\frac{n\tau_s}{\tau_b}\frac{\tau_{c20}}{\tau_c}\frac{\ln\left(1+A\dfrac{\tau_b}{\tau_{c20}}\right)}{\ln\left[\prod_{j=0}^{n-1}\left(\dfrac{1+A\dfrac{(n-j-1)\tau_p+j\tau_s}{(n-1)\tau_c}}{1+A\dfrac{(n-j-1)}{(n-1)}\dfrac{(\tau_p-\tau_s)}{\tau_c}}\right)\right]}. \tag{28}$$

Equation (28) suggests that it might be possible to increase the purpura threshold of a pulsed dye laser by increasing the number of subpulses. A typical 595 nm dye laser has a single pulse purpura threshold F_p around 5.2 J/cm^2 for τ_b =0.45 ms pulses. It is suggested that typically the clinical purpura is caused by overheating of blood vessels between 10 and 40 μm.[25] The compound pulse purpura threshold for a 595 nm laser with 0.1 ms subpulses is plotted on Fig. 9 as a function of the number of subpulses. The results suggest that if the only cause of clinical purpura is overheating of the small blood vessels then it is possible to build dye lasers with greatly increased purpura threshold.

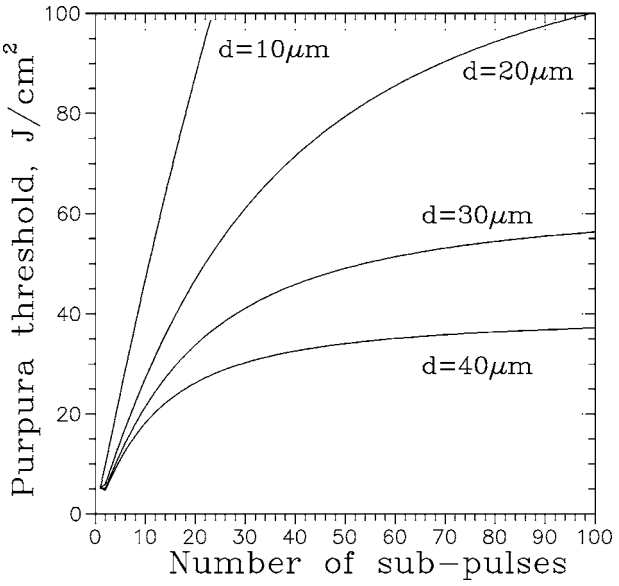

FIG. 9. Calculated purpura threshold radiant exposure versus number of subpulses with duration τ_s=0.1 ms, Eq. (28). Total pulse duration is fixed τ_p=40 ms. Wavelength=595 nm.

IX. EXPERIMENTAL RESULTS FOR PRACTICAL MULTIPULSE DYE LASERS

The analytical expression for the purpura threshold increase was compared with experimental data using a modified 595 nm V-Star laser from Cynosure Inc. The laser was set to produce compound pulses consisting of 3, 4, 5, or 6 equal amplitude subpulses equally spaced over a 40 ms total pulse duration. The radiant exposure delivered by the compound pulse was verified before and after each exposure.

Twenty-eight patients were involved in the study. Each patient was exposed to a series of laser pulses. All four laser pulse formats were investigated using a 7 mm spotsize. Also a single pulse 0.45 ms laser setting was used to determine the single pulse purpura threshold. All treatments were done on normal appearing skin in the buttocks region. Each treatment consisted of a series of 40 ms laser pulses whose radiant exposure was varied in steps of approximately 1 J/cm^2 up to the maximum radiant exposure available. One such series was carried out using each of the four available pulse formats. Digital photographs were taken at 24 h post treatment. By evaluating the photographs, the purpuric threshold was defined as the radiant exposure at which any nontransient redness or bruising was evident. A similar study using a laser with three subpulses has been published.[26]

The experimental data is plotted in Fig. 10 with the calculated purpura thresholds using Eq. (28) for 20, 30, and

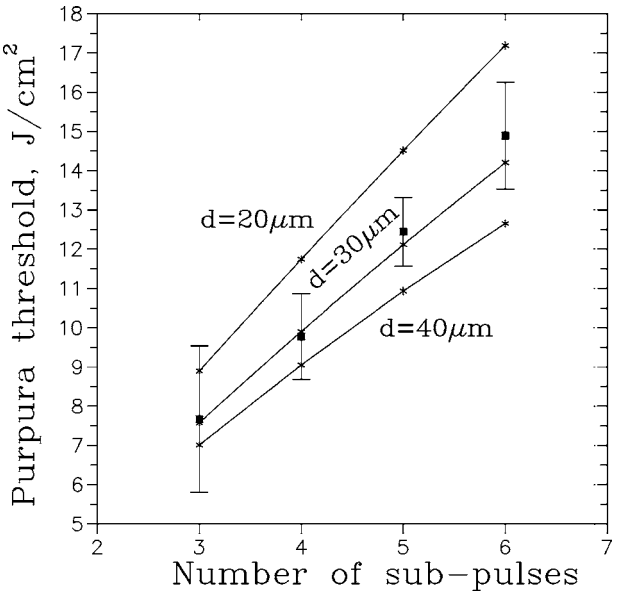

FIG. 10. Comparison of the theory, Eq. (28), with experimental data for purpura threshold radiant exposure versus number of subpulses with duration τ_s=0.1 ms. Total pulse duration is fixed τ_p=40 ms. Wavelength =595 nm.

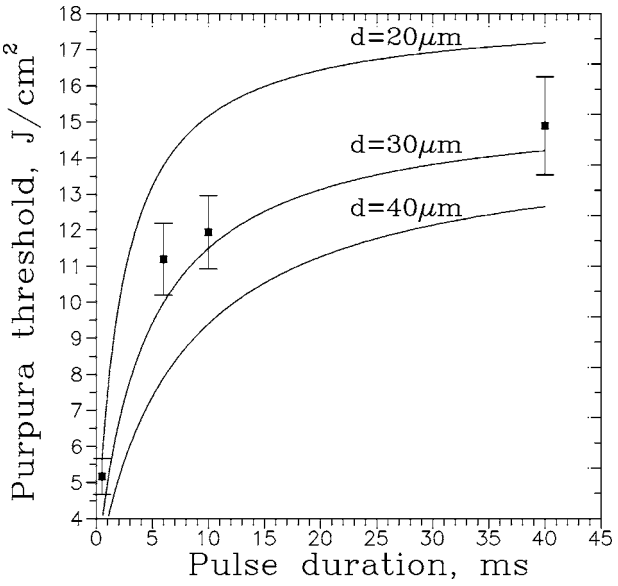

FIG. 11. Comparison of the theory, Eq. (28), with experimental data for purpura threshold radiant exposure versus total pulse duration τ_p. Data is taken for six equally spaced subpulses with duration τ_s=0.1 ms each. Wavelength=595 nm.

40 μm vessels. The calculated points are connected by solid lines for clarity. There is excellent agreement between the clinically observed purpura threshold and the calculations for blood vessels with diameters between 20 and 40 μm. The trend of increasing purpura threshold with increasing the number of subpulses is expected to continue as plotted in Fig. 9, however, the laser available for the study was limited to no more than six subpulses.

The purpura threshold of the 595 nm dye laser using a compound pulse consisting of six subpulses was evaluated also for compound pulse durations of 6 and 10 ms. The experimental data and the calculations for 20, 30, and 40 μm vessels are plotted in Fig. 11. The increase in the purpura threshold with increased pulse duration is evident both in the experimental data and the calculations.

A separate set of experiments were performed with a laser operating at 585 nm and delivering compound pulses consisting of six equally spaced 0.1 ms subpulses in a 7 mm spot. The purpura threshold tests were done on the buttocks skin of ten patients who volunteered to participate in the study. The experimental data and the calculations from Eq. (28) for the 585 nm laser study are plotted in Fig. 12. There is good agreement between the experimental data and the calculations for vessels between 20 and 30 μm. The purpura thresholds for the 585 nm laser are always lower than the 595 nm laser because of the much higher oxygenated blood absorption 165 cm^{-1} at 585 nm versus 36 cm^{-1} at 595 nm.[27,28] In both cases, cooling of the small blood vessels between subpulses leads to higher purpura threshold for longer pulses and the analytical model correctly predicts the increased purpura threshold.

X. DISCUSSION

While the treatment of vascular lesions is a complex and daunting problem, theoretical understanding of the use of a laser to address these indications begins with a thermal process analysis based on the tissue properties. It is remarkable that by means of a few simplifying assumptions, this initial step can be described by a very tractable and intuitive model. Often such models are applicable only over a very limited range of parameters; however, such is not the case here. In fact the model offers insight into the laser tissue response over a wide range of wavelengths, laser pulse formats, laser radiant exposure, and vascular dimensions. The applicability has been demonstrated by applying the model to the specific case of the analysis of the onset of purpura. The appearance of clinical purpura is usually an undesirable cosmetic side

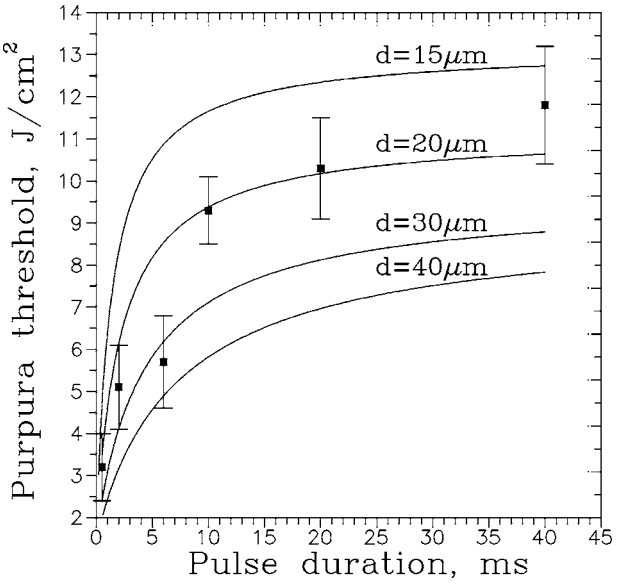

FIG. 12. Comparison of the theory, Eq. (28), with experimental data for purpura threshold radiant exposure versus total pulse duration τ_p. Data is taken for six equally spaced subpulses with duration τ_s=0.1 ms each. Wavelength=585 nm.

effect in dye laser clinical treatments. It has been shown here that the short term acute purpuric response can be described by the model resulting in simple formulas for the purpuric threshold as a function of the laser pulse structure. Clinical data gathered by the present authors as well as data from other experiments published over the last 20 years has been compared to the predictions of the model presented here. These data span more than three orders of magnitude of variation in laser parameters including pulse duration and peak power. In addition, the data include a variation in the laser wavelength that results in a factor of more than one order of magnitude in the absorption coefficient of oxyhemoglobin. In all cases, the predictions of the model are in excellent agreement with the experimental data.

The results of the application of the present thermal model to the onset of purpura not only predicts the threshold radiant exposure that yields purpura, but also yields insight into the size of the vessels involved in the process. As one might have anticipated, the model indicates that the shorter wavelengths (577 and 585 nm, Figs. 7 and 12) have a more profound effect on the smaller vessels than does the longer wavelength (Figs. 10 and 11). This is consistent with the higher blood absorption at the shorter wavelengths. A more detailed analysis of that effect will be included in a future refined theoretical model that will include the target absorption coefficient. In all cases, purpura is seen to be associated with the heating of vessels in the range of 20 to 30 μm diameter, consistent with histological data.[25]

This model provides a tool to guide the development of dye lasers. While the present analysis has dealt only with the comparison of model predictions with the onset of purpura, the ability to design a dye laser offering reduced risk of purpura while delivering radiant exposure capable of destroying larger unwanted vasculature is within the capability of the model. Recent publications[22–24] have reported such improved results, all consistent with the predictions of the model presented here.

While the work presented here has dealt only with the specific case of vascular malformation, the model is clearly applicable anytime the nature of the laser treatment is thermal. This is the case in many applications. One perhaps unique advantage when investigating vascular treatments is the existence of a very tractable and quantifiable marker, specifically the onset of purpura. Application of the model in cases where no such marker exists may be more difficult to verify through simple clinical experiments such as the ones presented here. Still, it is possible to obtain significant insight into these applications.

XI. CONCLUSION

An analytical model for laser pulse heating of embedded targets has been developed and verified for cylindrical targets for a wide range of laser absorption coefficients. Clinical purpura was used as a marker for small blood vessel damage under the assumption that purpura due to the same temperature rise in the vessel. Applying the model to experimental data published in the last 20 years validated the correspondence of small vessel temperature rise and purpuric appearance. The model uses only peak temperature as an indicator of tissue damage, avoids the calculation of thermal damage integrals involving empirical factors, and shows excellent agreement with experimental data for cylindrical targets. This analytical model leads to the derivation of analytical expressions that can be used to guide the development of future laser systems.

APPENDIX A: CYLINDRICAL TARGET GEOMETRY

The heat generation function of the form (3) is written in cylindrical geometry as

$$h(\vec{r}',t') = Q\Pi(t',\tau)\exp\left(-A\frac{x'^2+y'^2}{R^2}\right). \tag{A1}$$

The origin of the coordinate system is positioned in the center of the cylindrical target and z' is along the axis. The spatial portion of the integral in Eq. (2) can be expressed as a product of integrals over x', y', and z'.

$$T(\vec{r},t) = \int_{-\infty}^{t} dt' Q\Pi(t',\tau)\frac{I_x(t-t')I_y(t-t')I_z(t-t')}{8[\pi\alpha(t-t')]^{3/2}}. \tag{A2}$$

The initial step is integration over the spatial coordinates. The two integrals over x' and y' are identical, the z' integral has a different form because the heat generation function (A1) is independent of z'. The explicit form of the x' integral is

$$I_x = \int_{-\infty}^{\infty} dx' \exp\left[-\left(\frac{(x-x')^2}{\beta}\right)\right]\exp\left(-A\frac{x'^2}{R^2}\right),$$

where $\beta = 4\alpha(t-t')$.

The integral can be simplified to

$$I_x = \exp\left[\frac{(D-1)x^2}{\beta}\right]\int_{-\infty}^{\infty} dx' \exp\left[-\left(\frac{(x'-Dx)}{\sqrt{\beta D}}\right)^2\right]$$
$$= \sqrt{\pi\beta D}\exp\left[\frac{(D-1)x^2}{\beta}\right], \tag{A3}$$

where $D = R^2/(R^2+A\beta)$.

The solution (A3) is identical for the y' coordinate.

The explicit form of the z' integral is

$$I_z = \int_{-\infty}^{\infty} dz' \exp\left[-\left(\frac{(z-z')^2}{\beta}\right)\right] = \sqrt{\pi\beta} \tag{A4}$$

The integrals over x', y', and z' are substituted in the original integral expression to obtain

$$T(r,t) = \frac{Q}{\rho c}\int_{-\infty}^{t} dt'\Pi(t',\tau)D\exp\left[\frac{(D-1)r^2}{\beta}\right], \tag{A5}$$

where r is the radial coordinate in the cylindrical target, $r^2 = x^2+y^2$. Using the explicit expression for D, the integral (A5) reduces to

$$T(r,t) = \frac{QR^2}{\rho c}\int_{-\infty}^{t} dt' \Pi(t',\tau)\frac{1}{(R^2+A\beta)}\exp\left[-\frac{Ar^2}{R^2+A\beta}\right]. \tag{A6}$$

The next step is integration over the temporal coordinate. The temporal function of the rectangular heating pulse $\Pi(t',\tau)$ produces two expressions for the temperature variation with different forms during the heating and the cooling phase.

$$T(r,t) = \begin{cases} \dfrac{QR^2}{\rho c}\displaystyle\int_0^t dt' \frac{1}{(R^2+A\beta)}\exp\left[-\frac{Ar^2}{R^2+A\beta}\right], & t \le \tau \quad \text{(heating)} \\ \dfrac{QR^2}{\rho c}\displaystyle\int_0^\tau dt' \frac{1}{(R^2+A\beta)}\exp\left[-\frac{Ar^2}{R^2+A\beta}\right], & t > \tau \quad \text{(cooling)} \end{cases}. \tag{A7}$$

A change of variables based on the definition for β simplifies the integral $\beta = 4\alpha(t-t')$

$$T(r,t) = \begin{cases} \dfrac{QR^2}{\rho c}\displaystyle\int_{4\alpha t}^{0} \frac{1}{(R^2+A\beta)}\exp\left[-\frac{Ar^2}{R^2+A\beta}\right]\frac{-1}{4\alpha}d\beta, & t \le \tau \\ \dfrac{QR^2}{\rho c}\displaystyle\int_{4\alpha t}^{4\alpha(t-\tau)} \frac{1}{(R^2+A\beta)}\exp\left[-\frac{Ar^2}{R^2+A\beta}\right]\frac{-1}{4\alpha}d\beta, & t > \tau \end{cases}. \tag{A8}$$

The integrals can be simplified by the following change of variables $\xi = \frac{Ar^2}{R^2+A\beta}$

$$T(r,t) = \begin{cases} \dfrac{QR^2}{\rho c}\dfrac{1}{4\alpha A}\displaystyle\int_{Ar^2/[R^2+A4\alpha t]}^{A(r/R)^2} \frac{\exp[-\xi]}{\xi}d\xi, & t \le \tau \\ \dfrac{QR^2}{\rho c}\dfrac{1}{4\alpha A}\displaystyle\int_{Ar^2/[R^2+A4\alpha t]}^{Ar^2/[R^2+A4\alpha(t-\tau)]} \frac{\exp[-\xi]}{\xi}d\xi, & t > \tau \end{cases}. \tag{A9}$$

The integrals can be expressed in terms of exponential integrals $E_1(s)$

$$E_1(s) = \int_s^\infty \frac{\exp(-\xi)}{\xi}d\xi = -\gamma - \ln(s) - \sum_{n=1}^{\infty}\frac{(-1)^n s^n}{n!\,n}, \text{ where } \gamma = 0.57721.$$

Then the solution for the temperature distribution in a cylindrical target can be expressed as

$$T(r,t) = \begin{cases} \dfrac{QR^2}{\alpha\rho c}\dfrac{1}{4A}\left[E_1\left(\dfrac{Ar^2}{R^2+A4\alpha t}\right) - E_1\left(A\dfrac{r^2}{R^2}\right)\right], & t \le \tau \\ \dfrac{QR^2}{\alpha\rho c}\dfrac{1}{4A}\left[E_1\left(\dfrac{Ar^2}{R^2+A4\alpha t}\right) - E_1\left(\dfrac{Ar^2}{R^2+A4\alpha(t-\tau)}\right)\right], & t > \tau \end{cases} \tag{A10}$$

For a square pulse in time, the heat generation rate Q (J/m^3s) can be expressed as a ratio of the deposited energy density $q(J/m^3)$ and the pulse duration τ, $Q = q/\tau$. It is convenient to introduce also a characteristic time for the target $\tau_c = \frac{R^2}{4\alpha} = \frac{d^2}{16\alpha}$. The expression for the temperature distribution (A10) can be rearranged as

$$T(r,t) = \frac{q}{\rho c}\frac{\tau_c}{\tau}\frac{1}{A}\left[E_1\left(\frac{r^2}{R^2}\frac{A}{1+A\dfrac{t}{\tau_c}}\right) - E_1\left(\frac{r^2}{R^2}\frac{A}{1+A\dfrac{\langle t-\tau\rangle}{\tau_c}}\right)\right], \tag{A11}$$

where

$$\langle x\rangle = \begin{cases} x, & \text{for } x \ge 0 \\ 0, & \text{for } x < 0 \end{cases}$$

represents the Macauley bracket or ramp function.

The total amount of energy per unit length delivered to the target E can be calculated from the expression for the heat generation rate of a Gaussian heater (3)

$$E = \int_{-\infty}^{\tau} dt' \int_0^{2\pi} d\varphi \int_0^{\infty} r' dr' \frac{q}{\tau}\Pi(t',\tau)\exp\left(-A\frac{r'^2}{R^2}\right) = q\frac{\pi R^2}{A}. \tag{A12}$$

If the same target were heated by a source depositing uniform energy density u (J/m^3s), the energy per unit length delivered to the target would be

$$E_u = u\pi R^2 \tag{A13}$$

The expressions (A12) and (A13) for the total energy delivered to the target can be used to derive a relation between the uniform energy density u delivered to a target and the peak energy density in the center of the target q for an equivalent Gaussian source.

$$q = Au \tag{A14}$$

The energy density relationship (A14) can be substituted in the expression for the temperature variation (A11) to obtain an approximate formula for the temperature variation in a uniformly heated cylindrical target.

$$T(r,t) = \frac{u}{\rho c}\frac{\tau_c}{\tau}\left[E_1\left(\frac{r^2}{R^2}\frac{A}{1+A\dfrac{t}{\tau_c}}\right) - E_1\left(\frac{r^2}{R^2}\frac{A}{1+A\dfrac{\langle t-\tau\rangle}{\tau_c}}\right)\right] \tag{A15}$$

For the temperature in the center of the target the expression (A15) can be simplified using the series expansion for the exponential integral

$$T_C(t) = \frac{u}{\rho c}\frac{\tau_c}{\tau}\ln\left(\frac{1+A\dfrac{t}{\tau_c}}{1+A\dfrac{\langle t-\tau\rangle}{\tau_c}}\right). \tag{A16}$$

APPENDIX B: SPHERICAL TARGET GEOMETRY

Following the procedure outlined in Appendix A, the heat generation function of the form (3) is written in spherical geometry as

$$h(\vec{r}',t') = Q\Pi(t',\tau)\exp\left(-A\frac{x'^2+y'^2+z'^2}{R^2}\right) \tag{B1}$$

The origin of the coordinate system is positioned in the center of the spherical target. The spatial portion of the integral in Eq. (2) can be expressed as a product of integrals over x', y', and z'.

$$T(\vec{r},t) = \int_{-\infty}^{t} dt' Q\Pi(t',\tau)\frac{I_x(t-t')I_y(t-t')I_z(t-t')}{8[\pi\alpha(t-t')]^{3/2}} \tag{B2}$$

The initial step is integration over the spatial coordinates. The three integrals over x', y', and z' are identical. Their explicit form is shown in (A3). They are substituted in the original integral expression to obtain

$$T(r,t) = \frac{QR^3}{\rho c}\int_{-\infty}^{t} dt'\Pi(t',\tau)\frac{1}{(R^2+A\beta)^{3/2}} \times\exp\left[-\frac{Ar^2}{R^2+A\beta}\right], \tag{B3}$$

where r is the radial coordinate in the spherical target, $r^2 = x^2+y^2+z^2$, β is defined in Appendix A. The next step is integration over the temporal coordinate. The integral can be simplified by the following change of variables $\varphi = r\sqrt{A}/\sqrt{R^2+A\beta}$

$$T(r,t) = \begin{cases} \dfrac{QR^3}{\rho c}\dfrac{1}{2\alpha r A^{3/2}}\displaystyle\int_{r\sqrt{A}/\sqrt{R^2+A4\alpha t}}^{(r/R)\sqrt{A}} \exp[-\varphi^2]d\varphi, & t\le\tau \\ \dfrac{QR^3}{\rho c}\dfrac{1}{2\alpha r A^{3/2}}\displaystyle\int_{r\sqrt{A}/\sqrt{R^2+A4\alpha t}}^{r\sqrt{A}/\sqrt{R^2+A4\alpha(t-\tau)}} \exp[-\varphi^2]d\varphi, & t>\tau \end{cases}. \tag{B4}$$

The formula for the temperature variation in a uniformly heated spherical target becomes

$$T(r,t) = \frac{4}{3}\frac{u}{\rho c}\frac{\tau_c}{\tau}\frac{R}{r}\left[\operatorname{erf}\left(\frac{r}{R}\frac{\sqrt{A}}{\sqrt{1+A\dfrac{\langle t-\tau\rangle}{\tau_c}}}\right) - \operatorname{erf}\left(\frac{r}{R}\frac{\sqrt{A}}{\sqrt{1+A\dfrac{t}{\tau_c}}}\right)\right]. \tag{B5}$$

For the temperature in the center of the target, the expression (B5) can be simplified using the mean value theorem for the integrals in expression (B4)

$$T_C(t) = \frac{u}{\rho c}\frac{\tau_c}{\tau}\frac{8}{3}\sqrt{\frac{A}{\pi}}\left[\frac{1}{\sqrt{1+A\dfrac{\langle t-\tau\rangle}{\tau_c}}} - \frac{1}{\sqrt{1+A\dfrac{t}{\tau_c}}}\right] \tag{B6}$$

APPENDIX C: PLANAR TARGET GEOMETRY

Following the procedure outlined in Appendix A, the heat generation functions of the form (3) is written in planar geometry as

$$h(\vec{r}',t') = Q\Pi(t',\tau)\exp\left(-A\frac{x'^2}{R^2}\right) \tag{C1}$$

The origin of the coordinate system is positioned in the center of the planar target and x' is along the width of the target. The spatial portion of the integral in Eq. (2) can be expressed as a product of integrals over x', y', and z'.

$$T(\vec{r},t) = \int_{-\infty}^{t} dt' Q\Pi(t',\tau)\frac{I_x(t-t')I_y(t-t')I_z(t-t')}{8[\pi\alpha(t-t')]^{3/2}}. \tag{C2}$$

The initial step is integration over the spatial coordinates. The integral over x' is solved in Appendix A (A3). The two integrals over y' and z' are identical. Their explicit form is shown in (A4). They are substituted in the original integral expression to obtain

$$T(r,t) = \frac{QR}{\rho c}\int_{-\infty}^{t} dt'\Pi(t',\tau)\frac{1}{\sqrt{(R^2+A\beta)}}\exp\left[-\frac{Ax^2}{R^2+A\beta}\right], \tag{C3}$$

where β is defined in Appendix A.

The next step is integration over the temporal coordinate. The integrals can be simplified by the following change of variables $\varphi = x\sqrt{A}/\sqrt{R^2+A\beta}$

$$T(r,t) = \begin{cases} \dfrac{QR}{\rho c}\dfrac{x}{2\alpha\sqrt{A}}\displaystyle\int_{x\sqrt{A}/\sqrt{R^2+A4\alpha t}}^{(x/R)\sqrt{A}} \frac{\exp[-\varphi^2]}{\varphi^2}d\varphi, & t\le\tau \\ \dfrac{QR}{\rho c}\dfrac{x}{2\alpha\sqrt{A}}\displaystyle\int_{x\sqrt{A}/\sqrt{R^2+A4\alpha t}}^{x\sqrt{A}/\sqrt{R^2+A4\alpha(t-\tau)}} \frac{\exp[-\varphi^2]}{\varphi^2}d\varphi, & t>\tau \end{cases}. \tag{C4}$$

The formula for the temperature variation in a uniformly heated spherical target becomes

$$T(r,t)=\frac{u}{\rho c}\frac{\tau_c}{\tau}\frac{x}{R}\frac{4}{\sqrt{\pi}}\left[\begin{array}{l}\dfrac{\exp\left[-\dfrac{x^2}{R^2}\dfrac{A}{1+At/\tau_c}\right]}{\dfrac{x}{R}\dfrac{\sqrt{A}}{\sqrt{1+At/\tau_c}}}-\dfrac{\exp\left[-\dfrac{x^2}{R^2}\dfrac{A}{1+A\langle t-\tau\rangle/\tau_c}\right]}{\dfrac{x}{R}\dfrac{\sqrt{A}}{\sqrt{1+A\langle t-\tau\rangle/\tau_c}}}+\\ +\sqrt{\pi}\mathrm{erf}\left(\dfrac{x}{R}\dfrac{\sqrt{A}}{\sqrt{1+At/\tau_c}}\right)-\sqrt{\pi}\mathrm{erf}\left(\dfrac{x}{R}\dfrac{\sqrt{A}}{\sqrt{1+A\langle t-\tau\rangle/\tau_c}}\right)\end{array}\right]. \tag{C5}$$

For the temperature in the center of the target the expression (C5) can be simplified using the mean value theorem for the integrals in expression (C4)

$$T_C(t)=\frac{u}{\rho c}\frac{\tau_c}{\tau}\frac{4}{\sqrt{\pi A}}\left[\sqrt{1+A\frac{t}{\tau_c}}-\sqrt{1+A\frac{\langle t-\tau\rangle}{\tau_c}}\right]. \tag{C6}$$

APPENDIX D: SECOND ORDER CYLINDRICAL TARGET GEOMETRY

Following the procedure outlined in Appendix A, for the heat generation function of the form (11), the spatial portion of the integral in Eq. (2) can be expressed as a product of integrals of x', y', and z'. The initial step is integration over the spatial coordinates

$$T(\vec{r},t)=\int_{-\infty}^{t}dt'Q\Pi(t,\tau)\frac{I_{xy}(t-t')I_z(t-t')}{8[\pi\alpha(t-t')]^{3/2}}, \tag{D1}$$

where the I_{xy} integral is defined as

$$I_{xy}=\int_{-\infty}^{\infty}dy'\left[I_{x1}(t-t')+\frac{y'^2}{R^2}I_x(t-t')\right]\times\exp\left[-\left(\frac{(y-y')^2}{\beta}\right)\right]\exp\left(-A\frac{y'^2}{R^2}\right).$$

The integral I_x is solved in Appendix A (A3). The explicit form of the I_{x1} integral is

$$I_{x1}=\int_{-\infty}^{\infty}dx'\frac{x'^2}{R^2}\exp\left[-\left(\frac{(x-x')^2}{\beta}\right)\right]\exp\left(-A\frac{x'^2}{R^2}\right)=\exp\left[\frac{(D-1)x^2}{\beta}\right]\sqrt{\pi\beta D}\frac{D}{R^2}\left[\frac{\beta}{2}+Dx^2\right],$$

where β is defined in Appendix A.

The solution for the I_x and I_{x1} are substituted in the I_{xy} integral.

$$I_{xy}=\exp\left[\frac{(D-1)x^2}{\beta}\right]\sqrt{\pi\beta D}\int_{-\infty}^{\infty}dy'\left[\frac{D}{R^2}\left(\frac{\beta}{2}+Dx^2\right)+\frac{y'^2}{R^2}\right]\exp\left[-\left(\frac{(y-y')^2}{\beta}\right)\right]\exp\left(-A\frac{y'^2}{R^2}\right)$$

The I_{xy} integral can be done as a sum of two integrals I_{y1} and I_{y2}. Where the integral I_{y1} is similar to I_x and I_{y2} is similar to I_{x1}. The result is

$$I_{xy}=\exp\left[\frac{(D-1)(x^2+y^2)}{\beta}\right]\frac{\pi\beta D^2}{R^2}[\beta+D(x^2+y^2)].$$

The integral over z' is identical to the z' integral in Appendix A (A4).

The integrals I_{xy} and I_z can be substituted in the original integral expression (D1) to obtain

$$T(r,t)=\frac{QR^2}{\rho c}\int_{-\infty}^{t}dt'\Pi(\tau)\frac{1}{(R^2+A\beta)^2}\left[\beta+\frac{R^2r^2}{R^2+A\beta}\right]\times\exp\left[-\frac{Ar^2}{R^2+A\beta}\right]. \tag{D2}$$

The next step is integration over the temporal coordinate. The integral can be simplified by the following change of variables $\xi=Ar^2/(R^2+A\beta)$

$$T(r,t)=\begin{cases}\dfrac{QR^2}{\rho c}\dfrac{1}{4\alpha A^2}\displaystyle\int_{Ar^2/[R^2+A4\alpha t]}^{A(r/R)^2}\left[\frac{1}{\xi}+\frac{R^2}{Ar^2}(\xi-1)\right]\times\exp[-\xi]d\xi, & t\le\tau\\ \dfrac{QR^2}{\rho c}\dfrac{1}{4\alpha A^2}\displaystyle\int_{Ar^2/[R^2+A4\alpha t]}^{Ar^2/[R^2+A4\alpha(t-\tau)]}\left[\frac{1}{\xi}+\frac{R^2}{Ar^2}(\xi-1)\right]\times\exp[-\xi]d\xi, & t>\tau\end{cases}. \tag{D3}$$

Then the second order solution for the temperature distribution in a cylindrical target can be expressed as

$$T(r,t)=\frac{q}{\rho c}\frac{\tau_c}{\tau}\frac{1}{A^2}\left[\begin{array}{l}E_1\left(\dfrac{r^2}{R^2}\dfrac{A}{1+A\dfrac{t}{\tau_c}}\right)-E_1\left(\dfrac{r^2}{R^2}\dfrac{A}{1+A\dfrac{\langle t-\tau\rangle}{\tau_c}}\right)+\\ +\dfrac{1}{1+A\dfrac{t}{\tau_c}}\exp\left(-\dfrac{r^2}{R^2}\dfrac{A}{1+A\dfrac{t}{\tau_c}}\right)\\ -\dfrac{1}{1+A\dfrac{\langle t-\tau\rangle}{\tau_c}}\exp\left(-\dfrac{r^2}{R^2}\dfrac{A}{1+A\dfrac{\langle t-\tau\rangle}{\tau_c}}\right)\end{array}\right]. \tag{D4}$$

[1]T. J. Pfefer, J. K. Barton, D. J. Smithies, T. E. Milner, J. S. Nelson, M. J. van Gemert, and A. J. Welch, Lasers Surg. Med. **24**, 151 (1999).
[2]G. Shafirstein, W. Baumler, M. Lapidoth, S. Ferguson, P. E. North, and M. Waner, Lasers Surg. Med. **34**, 335 (2004).
[3]J. W. Tunnell, L. V. Wang, and B. Anvari, Appl. Opt. **42**, 1367 (2003).
[4]E. V. Ross and Y. Domankevitz, Lasers Surg. Med. **36**, 105 (2005).
[5]J. K. Barton, A. Rollins, S. Yazdanfar, T. J. Pfefer, V. Westphal, and J. A. Izatt, Phys. Med. Biol. **46**, 1665 (2001).
[6]C. T. Lahaye and M. J. van Gemert, Phys. Med. Biol. **30**, 573 (1985).
[7]W. F. Cheong, S. A. Prahl, and A. J. Welch, IEEE J. Quantum Electron. **26**, 2166 (1990).
[8]B. Choi, E. D. Jansen, and A. J. Welch, J. Appl. Phys. **94**, 7826 (2003).
[9]H. S. Carslaw and J. C. Jaeger, *Conduction of Heat in Solids* (Oxford University Press, New York, 1959).
[10]S. Gabay, I. Kremer, I. Ben-Sira, and G. Erez, Lasers Surg. Med. **8**, 418 (1988).
[11]D. J. Sanders, Appl. Opt. **23**, 30 (1984).
[12]S. L. Jacques and S. A. Prahl, Lasers Surg. Med. **6**, 494 (1987).
[13]M. J. van Gemert and A. J. Welch, Lasers Surg. Med. **9**, 405 (1989).
[14]L. J. Meijering, M. J. van Gemert, G. H. Gijsbers, and A. J. Welch, Lasers Surg. Med. **13**, 685 (1993).
[15]M. J. van Gemert, G. W. Lucassen, and A. J. Welch, Phys. Med. Biol. **41**, 1381 (1996).
[16]R. R. Anderson and J. A. Parrish, Lasers Surg. Med. **1**, 263 (1981).
[17]C. C. Dierickx, J. M. Casparian, V. Venugopalan, W. A. Farinelli, and R. R. Anderson, J. Invest. Dermatol. **105**, 709 (1995).
[18]W. Verkruysse, M. J. van Gemert, D. J. Smithies, and J. S. Nelson, Phys. Med. Biol. **45**, N197 (2000).
[19]C. R. Thompson, B. S. Gerstman, S. L. Jacques, and M. E. Rogers, Bull. Math. Biol. **58**, 513 (1996).
[20]E. J. Fiskerstrand, L. O. Svaasand, and J. S. Nelson, Lasers Surg. Med. **32**, 399 (2003).
[21]*Optical-Thermal Response of Laser-Irradiated Tissue*, edited by A. J. Welch and M. J. van Gemert (Plenum Press, Norwell, MA, 1995).
[22]E. Tanghetti, Lasers Surg. Med. **S15**, 95 (2003).
[23]J. R. Lloyd, Lasers Surg. Med. **S16**, 217 (2004).
[24]G. Munavalli, M. A. Weiss, K. L. Beasley, and R. A. Weiss, Lasers Surg. Med. **S17**, 250 (2005).
[25]J. M. Garden, O. T. Tan, R. Kerschmann, J. Boll, H. Furumoto, R. R. Anderson, and J. A. Parrish, J. Invest. Dermatol. **87**, 653 (1986).
[26]E. Tanghetti, R. A. Sierra, E. A. Sherr, and M. Mirkov, Lasers Surg. Med. **31**, 363 (2002).
[27]S. Prahl, Optical Absorption of Hemoglobin, http://omlc.ogi.edu/spectra/hemoglobin/index.html (1999).
[28]S. Jacques, Skin Optics, http://omlc.ogi.edu/news/jan98/skinoptics.html (1998).